Automatic Detection of Benign and Malignant Masses in Mammogram Using 2D-Fourier-BesselIntrinsic Band Functions and Improved Feature Space

Automatic Detection of Benign and Malignant Masses in Mammogram Using 2D-Fourier-Bessel Intrinsic Band Functions and Improved Feature Space

Pradeep Kumar Chaudhary and Ram Bilas Pachori *Senior Member, IEEE*

***Abstract*—This paper propose a framework based on 2D-Fourier-Bessel decomposition method (2D-FBDM) and improved feature space for automatic diagnosis of benign and malignant masses in mammogram. For analysis purpose, curated breast imaging subbset of digital database for screening mammography (CBIS-DDSM) is used. Haralick texture features are used to extract finesse, coarse or smoothness, and irregularities in 2D-Fourier-Bessel intrinsic band functions which are obtained by 2D-FBDM. Linear regression based improved feature space is produced and effects on classification performance are analysed after ensambling them with old feature space. For CBIS-DDSM the accuracy, sensitivity, specificity, and area under curve of receiver operating characteristic obtained by proposed framework is 97.48%, 97.16%, 97.86%, and 0.99 respectively. The mini-mammographic image analysis society database is also analysed to show robustness of proposed framework.**

***Index Terms*—Fourier-Bessel decomposition method (FBDM), Haralick texture feature, Improved feature space, Mammogram.**

I. Introduction

BREAST cancer is one of the most deadly cancers, accounting for 25% of new cases and 17% of cancer-related deaths in women globally. [1]. According to WHO, 2.1 million women suffer from breast cancer every year (in 2018) [2]. Most common way of screening breast cancer is through mammogram. Masses and microcalcification are the two most common signs of the diseases. Compared to microcalcification, masses are difficult to detect because masses occur at dense area of breast tissue, having smooth boundaries, and undefined shapes. Mammogram analysis is a difficult profession, because even well-trained experts might have a 65% to 75% interobserver variation rate. It was also discovered in that study that 65% to 90% of biopsies of suspected cancer were benign, highlighting the importance of developing computer-aided detection (CAD) techniques in conjunction with professional advice for early diagnosis [3]. In the same study it is also found that detection sensitivity without CAD was 80% and with CAD was 90%.

The most common abnormalities which are used in the literature is for masses detection. Masses with round or oval shape, low density, with well define boundaries are assumed as benign. Whereas masses with high density and ill defined shape and boundary are classified as malignant. In earlier works, the above defined features were used for automatic diagnosis of cancer (benign or malignant). The accuracy of such studies depends on the accuracy of mass segmentation which depends on threshold value and quality of mammogram [1]. Another analysis technique which is used in the literature is texture feature based breast cancer diagnosis. Because the mammogram is produced from a single medium of acquisition and the spatial distribution of features in these images can be identified within a single band, texture based feature has been proven to be beneficial in mammogram image analysis. Also texture feature evaluate finesse, coarse or smoothness, and irregularities in image which makes them suitable for classification of benign and malignant cancer [4]. In [5] authors have used gray-level co-occurrence matrix for extracting texture features and genetic algorithm for feature reduction followed by support vector (SVM) for classification. In [6] authors have first segmented boundaries of the lesion and then texture features were extracted from boundary region, interior of boundary region, and exterior of boundary region. Fractal descriptor, statistical descriptor and Haralick texture descriptor features where used in [7]. Similarly, various texture and shape where also used for breast cancer diagnosis [8]–[11]. The convolutional neural network (CNN) based breast cancer classification is a trending area. In [12] authors have proposed hybrid CNN model having two stages, first for preprocessing and other for supervised learning. In [13] different CNN models like VGG-16, ResNet-50, and inception V3 were trained on CBIS-DDSM using transfer learning approach and tested on INbrest database. A you only look once (YOLO) detector based CNN model was proposed in [14]. In [15] authors fused features extracted from VGG16, InceptionV3, and hand crafted texture features for classification of masses. In [16] authors used multiple region of interest (ROI) of masses, and each ROI are then passed to each ResNet-50 layers. The features from each ResNet-50 CNN are stacked with SVM to get final classification result. Although CNN based framework has shown good performance but has some disadvantages like if CNN is to be trained from the ground up, it will have high computational cost and require huge database for proper tuning of the model parameters. Transfer learning based approach can be the answer, but the resolution of the image has to be downsampled depending on the type of pretrained network used. It will have a negative impact on texture information

Pradeep Kumar Chaudhary and Ram Bilas Pachori are with Department of Electrical Engineering, Indian Institute of Technology Indore, Indore - 453552, India. (E-mail: phd1801202005@iiti.ac.in)

in the image, resulting in poor classification performance. [17]. Additionally, the dimension of the features obtained by the conventional machine learning based approaches is small. These features can be used by clinicians for diagnosis, which is not possible with CNN-based techniques. [17]. The signal decomposition techniques have also been used in diagnosis of breast cancer. In [18] authors have used wavelet and curvelets to get coefficients, followed by t-test to get reduced feature. In [19] authors have used discrete wavelet transform (DWT) and obtained angle cooccurrence matrix at different resolution. In [20] authors have applied trace transform (generalized Randon transform) functionals to extract features. The decomposition techniques like DWT, curvelet, Randon transform are non-adaptive, dyadic decomposition methods i.e. subimages obtained by such methods are independent of input image. In proposed work a new decomposition technique, 2D-Fourier-Bessel decomposition method (2D-FBDM) is introduced which is 2D extension of FBDM [21]. By adaptive decomposition, the subimages obtained are meaningful and the features obtained from those subimages are better than the features obtained by a single image and non-adaptive decomposed subimages. As the texture features has shown good classification performance specially Haralick texture descriptor feature. So in this work we have developed a framework based on 2D-FBDM and Haralick texture descriptor feature [4]. The main contributions of the work are as follows:

- Introduced new adaptive decomposition method, 2D-FBDM and used it to design a framework for automatic classification of masses in mammogram into benign and malignant.
- In proposed work, the performance of linear regression based improved feature space has been studied [22].
- Proposed framework is analyzed on two different database to check the robustness.

The remaining paper is organised as follows: section II briefly describes the databases, 2D-FBDM, and method to generate improved feature space using linear regression. In section III, proposed framework for automatic diagnosis of benign and malignant breast cancer from masses has been explained. In section IV simulation results are illustrated along with the discussions. Finally, the work is concluded in section V.

II. Database, 2D-FBDM, and linear regration based improved feature space

A. Database

In this work, we have used curated breast imaging subbset of digital database for screening mammography (CBIS-DDSM) [23] and mini-Mammographic Image Analysis Society (MIAS) database [24]. CBIS-DDSM consists of calcifications and masses abnormalities in full mammogram and ROI images in dicom format. For analysis of proposed framework, masses abnormalities of CBIS-DDSM have been used. The database has 1696 masses mammogram having two classes namely, benign (912) and malignant (784). The sample ROI of benign and malignant abnormalities of CBIS-DDSM is shown in Fig. 1. Database MIAS has been used for checking the robustness of the framework. MIAS have total 322 full mammogram (68 benign, 51 malignant, and 203 normal) of size (1024 $\times$ 1024) and in .pgm format. Dataset has also provided center and radii of the abnormalities, which is used to crop ROI from image of size 128$\times$128.

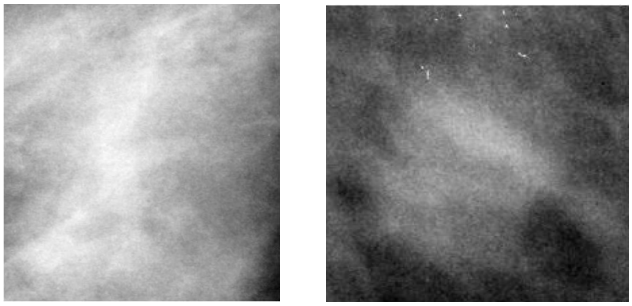

Fig. 1. ROI of Mammogram (a) Malignant and (b) Benign breast cancer.

B. 2D-FBDM

In [21], authors have proposed FBDM which decomposes a non-stationary multi-component signal into finite number of Fourier-Bessel intrinsic band functions (FBIBFs). This method is the modified version of Fourier decomposition method (FDM) [25] in which Fourier spectrum is replaced with Fourier-Bessel spectrum. The time-frequency representations (TFRs) obtained by FBDM gives better average normalized instantaneous resolution performance measure [26] as compared to FDM [21]. Motivated by results of FBDM and 2D extension of FDM [27], we are introducing 2D-FBDM.

The 2D-FBDM decomposes an image $I(x,y)$ into M number of 2D-FBIBFs $I_i(x,y)$ and a residue $R(x,y)$ [21], [27].

$$I(x,y) = \sum_{i=1}^{M} I_i(x,y) + R(x,y) \tag{1}$$

2D-FBIBF should be orthogonal to each other i.e. $\int_a^b \int_a^b I_i(x,y) I_j(x,y) dxdy = 0$ for $i \neq j$. The steps involved in 2D-FBDM are as follows:

- Apply FBSE row-wise followed by averaging along column. It will give average column spectrum. Similarly, apply FBSE column-wise followed by averaging along row, it will give average row spectrum. Analysis and synthesis equations of FBSE for signal $I(l)$ of length L are as follows [28], [29]:

$$I(l) = \sum_{x=1}^{L} C_x J_0\left(\frac{\varphi_x l}{L}\right), \qquad l = 0, 1, ..., L-1 \tag{2}$$

Where C_x represents FBSE coefficients, which can be expressed as [29],

$$C_x = \frac{2}{L^2 (J_1(\varphi_x))^2} \sum_{l=0}^{L-1} l I(l) J_0\left(\frac{\varphi_x l}{L}\right), \qquad x = 1, 2, ..., L \tag{3}$$

$J_0(.)$ and $J_1(.)$ are Bessel functions of order zero and order one, respectively. φ_x represents x^{th} positive root of equation $J_0(.) = 0$ [29].

- Compute row ($[\text{row}\omega_i]_{i=1}^{M1}$) and column ($[\text{column}\omega_i]_{i=1}^{M2}$) boundaries corresponding to average row spectrum and average column spectrum using FBDM [21]. Where $M1$ and $M2$ are number of row and column boundaries for FBIBF. To extract boundaries from obtained average row and column spectrum, first compute analytic Fourier-Bessel function (AFBF) $Z(l) = I(l) + j\hat{I}(l)$, where $I(l)$ is average row or column vector and $\hat{I}(l)$ is Hilbert transform of $I(l)$. $Z(l)$ can be expanded as,

$$Z(l) = \sum_{x=1}^{L} C_x J_0\left(\frac{\varphi_x l}{L}\right) + j\frac{1}{\pi l} * \sum_{x=1}^{L} C_x J_0\left(\frac{\varphi_x l}{L}\right) \quad (4)$$

where * represents convolution operation. Further $Z(l)$ can also be written as,

$$Z(l) = \sum_{i=1}^{M} a_i(l) e^{j\phi_i(l)} \quad (5)$$

Using (4) and (5) we can write as,

$$\sum_{i=1}^{M} a_i(l) e^{j\phi_i(l)} = \sum_{x=1}^{L} C_x J_0\left(\frac{\varphi_x l}{L}\right) + j\frac{1}{\pi l} * \sum_{x=1}^{L} C_x J_0\left(\frac{\varphi_x l}{L}\right) \quad (6)$$

Condition to obtain M FBIBFs on $Z(l)$ [21]: $a_i(l) \geq 0$, $\omega_i(t) = \frac{d\phi_i(l)}{dl} \geq 0, \forall l$. Where $\omega_i(l)$ and $a_i(l)$ are instantaneous frequency and instantaneous amplitude respectively of i^{th} AFBIBF. If scanning of condition is done from low to high frequency then process is named as low to high (LTH) frequency scanning (FS). Similarly, If scanning is performed from high frequency to low frequency then process is named as high to low (HTL) FS.
- Design row and column zero phase filter bank corresponding to row and column boundary frequencies [25].
- Filter image row-wise using row filter-bank followed by filtering column-wise using column filter-bank [30].
- Resultant will give $((M1+1)\times(M2+1))$ subband images or 2D-FBIBF. Apply Gram–Schmidt process to make all FBIBF orthogonal [27].

C. Linear regression based improved feature space

In [22], Amasyli has proposed linear regression based method to generate a improve feature space. From experimental results it has been concluded that by expanding the feature space (which is a combination of new feature set and old feature space) the base classifiers has shown better classification performance. The new feature space can be created by linear regression process which is as follows:

$$\text{AF} = [1' a\text{F}_i\text{F}_j]$$

$$b = (\text{AF}^T \times \text{AF})^{-1} \times \text{AF}^T \times \text{Tar} \quad (7)$$

$$gd = \text{AF} \times b$$

Where F_i and F_j are two randomly selected features from old feature set F. AF is a design matrix which can be designed based on parameter m= number of randomly selected features and n=order of matrix. For above equations (m,n)=(2,1). Tar and gd represent target and new feature space, respectively. Details of the methodology is well explained in [22]. The improved feature space is generated by adding new features with old features. The MATLAB source code of the method is available at https://github.com/ mfatihamasyali/improved_space.

III. Proposed methodology

Fig. 2 shows the work flow for automatic detection of malignant and benign from mammogram using 2D-FBDM and improved feature space.

In pre-processed step, contrast of input mammogram is improved using adaptive histogram equalization [30]. 2D-FBDM is used to decompose mammogram into subband images. 14 Haralick texture features are then extracted from each subband image, namely correlation (CORR), angular second moment (ASM), contrast (CON), sum of square (SOS), inverse difference moments (IDM), sum average (SA), sum entropy (SE), sum variance (SV), difference variance (DV), entropy (E), difference entropy (DE), information measure of correlation (IMC-1 and IMC-2), and maximal correlation coefficient (MCC) [31]. The significance of each feature and mathematical expression is well explained in [31] and MATLAB code for the same can be downloaded from https://in.mathworks.com/matlabcentral/fileexchange/58769-haralicktexturefeatures. Student's t-test is applied to extract significant features from obtained feature space [32]. The reduced feature space is then used to obtain improved feature space. For classification purpose we have used classification learner application of MATLAB (24 classifiers) and random forest (RF) [33] (as used in the experiment of [22]). Out of 24 classifiers, support vector machine (SVM) [34] and ensemble classifier has shown best performance, so only these two classifiers are shown in result section for performance comparison along with RF. The optimized parameters for SVM: The kernel function is Gaussian function and scale is 0.0048. The optimized parameters for ensemble classifier: ensemble method is gentle boost (GB) [35], number of learner is 50, and learning rate is 0.00146. The parameters mentioned are the best, as determined by the MATLAB's optimizable option. The number of trees in RF is set to 90 (obtained by trial and error method, keeping computational time and performance comparable to SVM and GB).

IV. Results and discussions

In this work, we evaluated proposed framework on CSIB-DDSM database. In first subsection, the simulation study has been carried out to find number of boundaries, best FS for FBDM (LTH or HTL), and number of features. In second subsection, performance evaluation is done on different values of m and n for linear regression based improved feature space. In third subsection, proposed method is also evaluated on MIAS database and performance of both MIAS and CSIB-DDSM databases is compared with different existing methods.

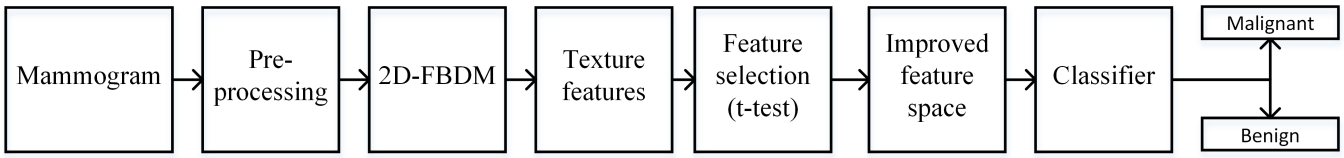

Fig. 2. Proposed framework for automated diagnosis of benign and malignant masses.

The performance parameters used are accuracy (ACC), sensitivity (SEN), specificity (SPE), and area under curve (AUC) of receiver operating characteristic [30].

The CSIB-DDSM database has provided separate database for training (1318) and testing (378). We have considered the same in our work so that we can easily compare our work with other existing work. The implementation of the methods is performed on MATLAB 2021b. The setup of the system is as follows: Dell Optiplex 790 computer with Intel Core i5 processor (3.20 GHz) and 14 GB RAM.

A. Parameter selection for FBDM method

The input ROI image is decomposed using FBDM both using LTH-FS and HTL-FS. Since the major information in images is available in low frequency region, so for both LTH and HTL-FS, boundaries are considered in increasing order of frequencies. Table. I shows the classification performance of HTL and LTH-FS for different number of boundaries. LTH-FS has shown marginally better performance than HTL-FS, as both approaches gives approximately same boundaries. The best performance is obtained by LTH-FS at number of boundaries=2 and by using RF classifier (shown with bold entries in Table. I). Fig. 3 shows the subband images for malignant and benign case obtained using LTH-FS for two boundaries [4]. The first subband image is known as approximate component (low frequency subband) and all other subband images are known as detail components (high frequency subband images). The approximate subband is a smooth version of input image which will help in extracting smoothness information present in the image. The detail subband will have the information related to sudden change in the image i.e. it will highlight irregularities and boundaries information present in the images. So the texture features will help in extracting such information from decomposed subband images. 14 Haralick texture features are extracted from each subband image. Since number of subband for number of boundaries equal to 2 are 9, So total number of features will be 126. Student's t-test is used reduce the features. Fig. 4 shows the plot for accuracy verses number of features, where features are arranged according to the p-value (obtained using Student's t-test). The best accuracy (82.47%) is obtained at 20 number of features and the features are: SA_5 $(3.52e{-}20)$, SOS_5 $(2.32e{-}15)$, MCC_1 $(2.38e{-}12)$, SOS_9 $(3.22e-11$, SA_3 $(8.22e-10)$, SOS_3 $(9.22e-9))$, SA_9 $(6.22e-9)$, SA_7 $(6.82e-8)$, SOS_7 $(9.22e-7)$, SA_4 $(9.12e-7)$, SOS_4 $(7.22e-7)$, SE_9 $(3.53e-7)$, IMC-2_4 $(5.23e-6)$, IDM_4 $(4.67e-6)$, E_4 $(5.72e-5)$, SE_4 $(3.8e-5)$, MCC_4 $(2.9e-5)$, $CORR_4$ $(2.3e-5)$, CON_4 $(8.2e-4)$, and DV_4 $(5.2e-4)$, where subscript represents subband image number and value inside bracket represents p-value of the respective feature. From Table I and Fig. 4, it can be concluded that for proposed framework, RF has shown better performance.

B. Parameter selection for improved feature space

The obtained features space has 20 number of features. Parameter m can be taken from 2, 4, . . ., $2 \times \log_2 d$ (d = number of features of old feature space). We use parameter n=1 and 2 because, the bigger the value, the higher will be the training time [22]. Here $d = 20$, so m can take value 2, 4, 6, 8, and 10. Table II shows performance comparison of old features with new improved ensemble features at different values of m and n. From Table II we can see that the best accuracy has been obtained for $m = 6$ and $n = 2$.

Performance of proposed framework is compared with no decomposition (same as proposed framework but without 2D-FBDM step), no contrast enhancement (same as proposed framework but without preprocessing), 2D-FDM [27] and with order-one 2D-FBDM based approach (same as proposed framework but instead of order-zero 2D-FBSE, order-one 2D-FBSE is used in 2D-FBDM [17]) in Table III. Table III also compares the computational time to classify single image and the tuned parameters. Bold entries show the best results obtained while comparison, proposed framework has shown best ACC, SEN, SPE, and AUC. No decomposition based method has least computational time, reason is that it does not use 2D-FBDM (2D-FBDM takes 1.100s to decompose single image). Also compare to 2D-FDM the 2D-FBDM is computationally complex reasion is the use of fast Fourier transform for implementation of 2D-FDM. Although the 2D-FBDM has shown better classification result, the reason may that the subband images obtained from 2D-FBDM is more meaning full as it uses FBSE (non-stationary basis for representing non-stationary signal) [21], [28].

C. Performance comparison of proposed framework

To check the reliability of proposed framework, the MIAS database has been used. We have used all five abnormalities in MIAS database: calcification, spiculated masses, architectural distortion, asymmetry, and other ill-defined masses and total three classes: benign, malignant, and normal. For this application we have used 10-fold cross-validation.

The performance comparison of proposed framework for both CBIS-DDSM and MIAS databases with other existing framework (CNN based texture feature based) is shown in Table IV. For CBIS-DDSM database, the proposed framework has given better performance than the CNN based approaches [13], [36], [38], [39], [42]. In [36], authors used bag of visual

TABLE I
PERFORMANCE COMPARISON OF LTH-FS AND HTL-FS OF 2D-FBDM AT DIFFERENT NUMBER OF BOUNDARIES USING RF, SVM, AND ENSEMBLE CLASSIFIER.

FS	Number of boundaries	RF				SVM				Ensemble			
		ACC	SEN	SPE	AUC	ACC	SEN	SPE	AUC	ACC	SEN	SPE	AUC
LTH	1	69	69.61	68.49	0.79	70.35	67.18	76.36	0.80	75.37	78.74	72.29	0.845
	2	**80.65**	**80.21**	81.18	**0.88**	79.5	71.74	**100**	0.87	80.60	79.08	82.04	0.88
	3	78.51	80.05	76.92	0.86	77.26	70.67	93.48	0.85	79.14	80.29	77.92	0.87
	4	77.26	79.55	75	0.85	76.31	70.46	89.69	0.851	75.37	78.74	72.29	0.84
HTL	1	68.82	69.37	68.22	0.785	70.35	67.18	76.36	0.80	78.64	85.51	73.39	0.860
	2	80.23	80	80.60	0.88	77.88	70.52	97.67	0.96	79.77	81.28	78.21	0.88
	3	76	78.28	73.75	0.84	76	69.79	91.30	0.84	77.26	78.82	75.64	0.85
	4	76	78.28	73.75	0.84	75.06	69.56	87.63	0.84	74.12	77.43	71.08	0.83

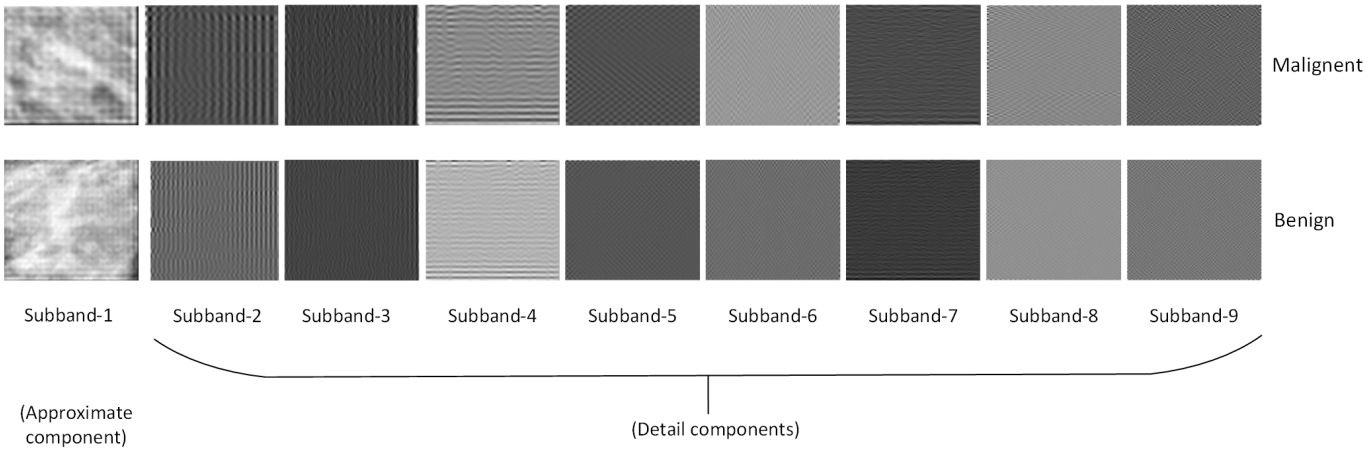

Fig. 3. Subband images for malignant and benign masses using LTH-FS 2D-FBDM.

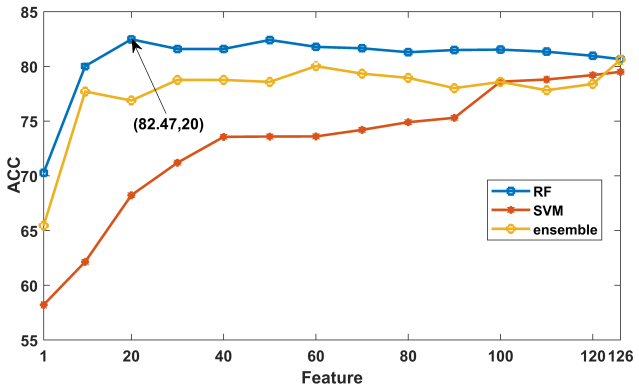

Fig. 4. Accuracy of RF, SVM, and ensemble classifier with different number of features.

TABLE II
PERFORMANCE COMPARISON OF IMPROVED FEATURE SPACE (AT DIFFERENT VALUE OF m AND n) WITH OLD FEATURE SPACE.

Feature space	ACC (%)	SEN (%)	SPE (%)	AUC
Old feature	82.47	82.45	82.50	0.920
$m = 2, n = 1$	89	89.98	88.33	0.973
$m = 2, n = 2$	88.69	88.26	89.13	0.972
$m = 4, n = 1$	89.76	89.19	90.44	0.975
$m = 4, n = 2$	93.40	92.35	94.69	0.990
$m = 6, n = 1$	92.90	91.46	94.39	0.988
$m = 6, n = 2$	**97.48**	**97.16**	**97.86**	**0.99**
$m = 8, n = 1$	93.27	92.25	94.09	0.987
$m = 8, n = 2$	96.29	96.01	96.64	0.99
$m = 10, n = 1$	93.84	93.47	94.23	0.99
$m = 10, n = 2$	95.72	94.94	96.68	0.99

words with CNN for both segment-free and segment dependent based classification and the segment-free based method has shown better performance. In [13], authors have compared the classification performance for three CNNs namely, VGG 16, ResNet-50, and Inception V3 and Inception V3 has shown best performance. In [38], region growing algorithm has been used for mass segmentation, and texture and shape features for feature extraction. Genetic algorithm is used for feature selection followed by artificial neural network (ANN) for classification. In [39] authors has used both texture features (feature like local binary pattern, global image descriptor, and histogram of oriented grading) and deep features from DenseNet and VGG. In [42] authors have used DWT (level-2) and extracted features from detail subband images. Finally, CNN is used for classification. The proposed method has outperformed above mention CNN method even though it is considered that CNN based methods are better than handful feature based methods. The reason may be that proposed work decomposes image into subband images where the first subband image is approximate subband image and all other subband images are detail components. So texture features

TABLE III
PERFORMANCE COMPARISON OF PROPOSED METHODS WITH NO DECOMPOSITION, NO CONTRAST ENHANCEMENT, 2D-FDM, AND ORDER-ONE 2D-FBDM.

Methods	FS	Boundaries	Feature	m and n	Classifier	ACC	SEN	SPE	AUC	Time
No decomposition	-	-	40	$m = 9$ and $n = 2$	Ensemble	83.15	81.78	84.49	0.92	**0.107s**
No contrast enhancement	LTH	2	25	$m = 6$ and $n = 2$	RF	96.78	97.01	96.52	0.98	1.192s
2D-FDM	LTH	2	30	$m = 6$ and $n = 2$	RF	96.87	93.21	96.59	0.98	1.029s
Order-one 2D-FBDM	LTH	2	20	$m = 6$ and $n = 2$	RF	97.03	96.80	97.30	0.99	1.149s
Proposed framework	LTH	2	20	$m = 6$ and $n = 2$	RF	**97.48**	**97.16**	97.86	**0.99**	1.149s

TABLE IV
COMPARISON OF PROPOSED FRAMEWORK FOR CBIS-DDSM AND MIAS DATABASE WITH EXISTING METHODS.

Reference	Methodology	ACC	SEN	SPE	AUC
	CBIS-DDSM				
[36]	Bag of visual words with CNN	-	-	-	0.86
[13]	Inception-V3 (Transfer learning)	84.16	-	-	0.93
[37]	Texture and shape feature with ANN	96.47	96.87	95.94	-
[38]	Deep neural network	79.60	-	-	0.87
[39]	Texture feature and deep features from residual network, DenseNet, and VGG with ensemble learners	90.91	82.96	**98.38**	0.983
[40]	Texture and shape feature with support vector machine	90.44	-	-	0.9
[41]	Gray-level co-occurrence matrix features with support vector machine	63.03		89.01	
[42]	DWT with CNN	88	-	-	0.93
	Proposed framework	**97.48**	**97.16**	97.86	**0.99**
	MIAS				
[43]	DWT with SVM	82.85	83.10	82.60	-
[44]	Gray-level co-occurrence matrix features from DWT subband and neural network	94.2	100	90	**0.95**
[45]	first order moment features curvelet transform subband images and with K-nearest neighbour	91.27	-	-	-
	Proposed framework	**96.06**	91.92	**95.64**	**0.95**

which will be obtained from approximate subband image, will evaluate finesse, coarse or smoothness in image and texture features from detail subband image evaluate irregularities and boundaries information in images. All these details from image can help in differentiating benign from malignant cancer, on the other hand, there is no clue about what kind of features are obtained by CNN based method. Another reason may be that, in proposed framework there is no need of resizing, in contrast, CNN based method (transfer learning) has to undergo forceful resizing (specially downsampling) which will directly affect resolution of image and reduce classification performance. For MIAS database, works [43]–[45] have used similar approach as done in proposed work. The reason that proposed work has shown better results is that the proposed decomposition technique is data adaptive and improved features space has boost classification performance.

For MIAS database, the proposed framework has provided 96.06% ACC, 91.92% average SEN, 95.64, average SPE 0.95, and 0.96 AUC. The average SEN and SPE can be obtained by weighted averaging SEN and SPE of all classes. The high ACC indicates robustness of the proposed method over existing works and hence it can be used for any application where texture information can be used for classification.

V. CONCLUSION

In this work, we have proposed a new 2D image decomposition technique, 2D-FBDM and used it to develop a framework for automatic diagnosis of benign and malignant from mammogram. We also studied the effects of using improved feature space at different values of m and n. For CBIS-DDSM the LTH-FS (at two number of boundaries) with $m = 6$ and $n = 2$ has shown better performance using RF classifier. The ACC, SEN, SPE, and AUC obtained by proposed framework are 97.48%, 97.16%, 97.86%, 0.99 respectively.

The results show that proposed framework can be used for automatic diagnosis of benign and malignant cancer from mammogram. The robustness of the methodology is justified with performance obtained on MIAS database, So the proposed framework can be used for other biomedical applications.

REFERENCES

[1] R. Rabidas, A. Midya, and J. Chakraborty, "Neighborhood structural similarity mapping for the classification of masses in mammograms," *IEEE Journal of Biomedical and Health Informatics*, vol. 22, no. 3, pp. 826–834, 2017.

[2] A. V. Vedalankar, S. S. Gupta, and R. R. Manthalkar, "Addressing architectural distortion in mammogram using alexnet and support vector machine," *Informatics in Medicine Unlocked*, vol. 23, p. 100551, 2021.

[3] P. Skaane, K. Engedal, and A. Skjennald, "Interobserver variation in the interpretation of breast imaging: comparison of mammography, ultrasonography, and both combined in the interpretation of palpable noncalcified breast masses," *Acta Radiologica*, vol. 38, no. 4, pp. 497–502, 1997.

[4] K. Ganesan, U. R. Acharya, C. K. Chua, L. C. Min, K. T. Abraham, and K.-H. Ng, "Computer-aided breast cancer detection using mammograms: a review," *IEEE Reviews in Biomedical Engineering*, vol. 6, pp. 77–98, 2012.

[5] H. Ketabi, A. Ekhlasi, and H. Ahmadi, "A computer-aided approach for automatic detection of breast masses in digital mammogram via spectral clustering and support vector machine," *Physical and Engineering Sciences in Medicine*, vol. 44, no. 1, pp. 277–290, 2021.

[6] C. Varela, S. Timp, and N. Karssemeijer, "Use of border information in the classification of mammographic masses," *Physics in Medicine & Biology*, vol. 51, no. 2, p. 425, 2006.

[7] B. Swiderski, S. Osowski, J. Kurek, M. Kruk, I. Lugowska, P. Rutkowski, and W. Barhoumi, "Novel methods of image description and ensemble of classifiers in application to mammogram analysis," *Expert Systems with Applications*, vol. 81, pp. 67–78, 2017.

[8] A. R. Domínguez and A. K. Nandi, "Toward breast cancer diagnosis based on automated segmentation of masses in mammograms," *Pattern Recognition*, vol. 42, no. 6, pp. 1138–1148, 2009.

[9] G. Vani, R. Savitha, and N. Sundararajan, "Classification of abnormalities in digitized mammograms using extreme learning machine," in *2010 11th International Conference on Control Automation Robotics & Vision*. IEEE, 2010, pp. 2114–2117.

[10] M. Fraschini, "Mammographic masses classification: novel and simple signal analysis method," *Electronics letters*, vol. 47, no. 1, pp. 14–15, 2011.

[11] W. J. Singh and B. Nagarajan, "Automatic diagnosis of mammographic abnormalities based on hybrid features with learning classifier," *Computer methods in biomechanics and biomedical engineering*, vol. 16, no. 7, pp. 758–767, 2013.

[12] J. Arevalo, F. A. González, R. Ramos-Pollán, J. L. Oliveira, and M. A. G. Lopez, "Representation learning for mammography mass lesion classification with convolutional neural networks," *Computer Methods and Programs in Biomedicine*, vol. 127, pp. 248–257, 2016.

[13] R. Agarwal, O. Diaz, X. Lladó, M. H. Yap, and R. Martí, "Automatic mass detection in mammograms using deep convolutional neural networks," *Journal of Medical Imaging*, vol. 6, no. 3, p. 031409, 2019.

[14] M. A. Al-Antari, S.-M. Han, and T.-S. Kim, "Evaluation of deep learning detection and classification towards computer-aided diagnosis of breast lesions in digital x-ray mammograms," *Computer Methods and Programs in Biomedicine*, vol. 196, p. 105584, 2020.

[15] M. Busaleh, M. Hussain, H. A. Aboalsamh, F.-e. Amin *et al.*, "Breast mass classification using diverse contextual information and convolutional neural network," *Biosensors*, vol. 11, no. 11, p. 419, 2021.

[16] I. Domingues, E. Sales, J. Cardoso, and W. Pereira, "Inbreast-database masses characterization," *XXIII CBEB*, 2012.

[17] P. K. Chaudhary and R. B. Pachori, "Automatic diagnosis of different grades of diabetic retinopathy and diabetic macular edema using 2-D-FBSE-FAWT," *IEEE Transactions on Instrumentation and Measurement*, 2022.

[18] M. M. Eltoukhy, I. Faye, and B. B. Samir, "A statistical based feature extraction method for breast cancer diagnosis in digital mammogram using multiresolution representation," *Computers in Biology and Medicine*, vol. 42, no. 1, pp. 123–128, 2012.

[19] A. Midya and J. Chakraborty, "Classification of benign and malignant masses in mammograms using multi-resolution analysis of oriented patterns," in *2015 IEEE 12th International Symposium on Biomedical Imaging (ISBI)*. IEEE, 2015, pp. 411–414.

[20] K. Ganesan, U. R. Acharya, C. K. Chua, C. M. Lim, and K. T. Abraham, "One-class classification of mammograms using trace transform functionals," *IEEE Transactions on Instrumentation and Measurement*, vol. 63, no. 2, pp. 304–311, 2013.

[21] V. Gupta and R. B. Pachori, "FBDM based time-frequency representation for sleep stages classification using EEG signals," *Biomedical Signal Processing and Control*, vol. 64, p. 102265, 2021.

[22] M. F. Amasyali, "Improved space forest: A meta ensemble method," *IEEE Transactions on Cybernetics*, vol. 49, no. 3, pp. 816–826, 2018.

[23] R. S. Lee, F. Gimenez, A. Hoogi, K. K. Miyake, M. Gorovoy, and D. L. Rubin, "A curated mammography data set for use in computer-aided detection and diagnosis research," *Scientific data*, vol. 4, no. 1, pp. 1–9, 2017.

[24] P. SUCKLING J, "The mammographic image analysis society digital mammogram database," *Digital Mammo*, pp. 375–386, 1994.

[25] P. Singh, S. D. Joshi, R. K. Patney, and K. Saha, "The Fourier decomposition method for nonlinear and non-stationary time series analysis," *Proceedings of the Royal Society A: Mathematical, Physical and Engineering Sciences*, vol. 473, no. 2199, p. 20160871, 2017.

[26] B. Boashash and V. Sucic, "Resolution measure criteria for the objective assessment of the performance of quadratic time-frequency distributions," *IEEE Transactions on Signal Processing*, vol. 51, no. 5, pp. 1253–1263, 2003.

[27] P. Singh and S. D. Joshi, "Some studies on multidimensional Fourier theory for Hilbert transform, analytic signal and AM–FM representation," *Circuits, Systems, and Signal Processing*, vol. 38, no. 12, pp. 5623–5650, 2019.

[28] J. Schroeder, "Signal processing via Fourier-Bessel series expansion," *Digital Signal Processing*, vol. 3, no. 2, pp. 112–124, 1993.

[29] R. B. Pachori and P. Sircar, "EEG signal analysis using FB expansion and second-order linear TVAR process," *Signal Processing*, vol. 88, no. 2, pp. 415–420, 2008.

[30] P. K. Chaudhary and R. B. Pachori, "Automatic diagnosis of glaucoma using two-dimensional Fourier-Bessel series expansion based empirical wavelet transform," *Biomedical Signal Processing and Control*, vol. 64, p. 102237, 2021.

[31] R. M. Haralick, K. Shanmugam, and I. H. Dinstein, "Textural features for image classification," *IEEE Transactions on Systems, Man, and Cybernetics*, no. 6, pp. 610–621, 1973.

[32] K. Das and R. B. Pachori, "Schizophrenia detection technique using multivariate iterative filtering and multichannel EEG signals," *Biomedical Signal Processing and Control*, vol. 67, p. 102525, 2021.

[33] V. F. Rodriguez-Galiano, B. Ghimire, J. Rogan, M. Chica-Olmo, and J. P. Rigol-Sanchez, "An assessment of the effectiveness of a random forest classifier for land-cover classification," *ISPRS Journal of Photogrammetry and Remote Sensing*, vol. 67, pp. 93–104, 2012.

[34] R.-E. Fan, P.-H. Chen, C.-J. Lin, and T. Joachims, "Working set selection using second order information for training support vector machines." *Journal of Machine Learning Research*, vol. 6, no. 12, 2005.

[35] P. Yin, A. Criminisi, J. Winn, and I. Essa, "Tree-based classifiers for bilayer video segmentation," in *2007 IEEE Conference on Computer Vision and Pattern Recognition*. IEEE, 2007, pp. 1–8.

[36] R. S. Lee, J. A. Dunnmon, A. He, S. Tang, C. Re, and D. L. Rubin, "Comparison of segmentation-free and segmentation-dependent computer-aided diagnosis of breast masses on a public mammography dataset," *Journal of Biomedical Informatics*, vol. 113, p. 103656, 2021.

[37] R. Rouhi, M. Jafari, S. Kasaei, and P. Keshavarzian, "Benign and malignant breast tumors classification based on region growing and CNN segmentation," *Expert Systems with Applications*, vol. 42, no. 3, pp. 990–1002, 2015.

[38] X. Shu, L. Zhang, Z. Wang, Q. Lv, and Z. Yi, "Deep neural networks with region-based pooling structures for mammographic image classification," *IEEE Transactions on Medical Imaging*, vol. 39, no. 6, pp. 2246–2255, 2020.

[39] H. Zhang, R. Wu, T. Yuan, Z. Jiang, S. Huang, J. Wu, J. Hua, Z. Niu, and D. Ji, "De-ada*: A novel model for breast mass classification using cross-modal pathological semantic mining and organic integration of multi-feature fusions," *Information Sciences*, vol. 539, pp. 461–486, 2020.

[40] I. A. Lbachir, I. Daoudi, and S. Tallal, "Automatic computer-aided diagnosis system for mass detection and classification in mammography," *Multimedia Tools and Applications*, vol. 80, no. 6, pp. 9493–9525, 2021.

[41] S. J. A. Sarosa, F. Utaminingrum, and F. A. Bachtiar, "Mammogram breast cancer classification using gray-level co-occurrence matrix and support vector machine," in *2018 International Conference on Sustainable Information Engineering and Technology (SIET)*. IEEE, 2018, pp. 54–59.

[42] M. Jasionowska and A. Gacek, "Wavelet convolution neural network for classification of spiculated findings in mammograms," in *International Conference on Information Technologies in Biomedicine*. Springer, 2019, pp. 199–208.

[43] F. Liu and M. Brown, "Breast cancer recognition by support vector machine combined with daubechies wavelet transform and principal component analysis," in *International Conference on ISMAC in Computational Vision and Bio-Engineering*. Springer, 2018, pp. 1921–1930.

[44] S. Beura, B. Majhi, and R. Dash, "Mammogram classification using two dimensional discrete wavelet transform and gray-level co-occurrence matrix for detection of breast cancer," *Neurocomputing*, vol. 154, pp. 1–14, 2015.

[45] S. Dhahbi, W. Barhoumi, and E. Zagrouba, "Breast cancer diagnosis in digitized mammograms using curvelet moments," *Computers in Biology and Medicine*, vol. 64, pp. 79–90, 2015.